IEEE Access
Multidisciplinary | Rapid Review | Open Access Journal

Received August 6, 2020, accepted August 14, 2020, date of publication August 18, 2020, date of current version August 31, 2020.

*Digital Object Identifier 10.1109/ACCESS.2020.3017492*

# Comprehensive Analysis of Side-Placed Metamaterials in Wireless Power Transfer System

**CONGHUI LU, XIUTAO HUANG, XIONG TAO, CANCAN RONG, (Member, IEEE), AND MINGHAI LIU**

School of Electrical and Electronic Engineering, Huazhong University of Science and Technology, Wuhan 430074, China

Corresponding author: Minghai Liu (mhliu@hust.edu.cn)

This work was supported in part by the National Key Research and Development Program of China under Grant 2018YFB0106300.

**ABSTRACT** In this article, we propose the side-placed negative-permeability metamaterial (NPM) and zero-permeability metamaterial (ZPM) in the wireless power transfer (WPT) system to simultaneously enhance the level of efficiency and meet the electromagnetic field (EMF) safety regulations. A theoretical analysis, simulation, and experiment are conducted to verify the feasibility of the proposed system model. Based on the principle of magneto-inductive waves (MIWs) and the shielding theory, the transmission characteristics of the WPT system without and with two NPM slabs, two ZPM slabs, and the combination of NPM and ZPM slabs are analyzed. The results demonstrate that the ZPM slabs and the combination of NPM and ZPM slabs have a high efficiency improvement when the transfer distance is located under 40 cm and exceeds 40 cm, respectively. Both methods can control the EMF leakage. Moreover, the side-placed metamaterial exhibits tolerance to the misalignment of the coil. Finally, comparative studies on the ZPM slab and aluminum are carried out. The experimental and simulation results show that the ZPM slab performs better than aluminum.

**INDEX TERMS** Zero-permeability, negative-permeability, combination, increase efficiency, shield magnetic field, MIW, wireless power transfer (WPT).

## I. INTRODUCTION

With the constant development of the electrification of society, consumer devices have become more popular, meanwhile, new requirements for charging methods have emerged. Wireless power transfer (WPT) can charge devices contactless, which introduces great convenience to users [1]. Since 2007, MIT has proposed WPT technology via coupled magnetic resonance, and it has become a popular research topic in recent years [2]. Wireless charging techniques have shown great potential in medical devices [3], internet of things (IOT) devices [4], mobile devices [5], and electric vehicles [6].

However, WPT technology still has a series of technical bottlenecks, such as low transfer efficiency and high magnetic field leakage. For instance, when the transfer distance increases and the coil misalignment, results in a lower transfer efficiency. In addition, the problem of electromagnetic field (EMF) leakage has become increasingly prominent in power transmission. These challenges can prevent the further development of WPT technology [7]. Therefore, a tradeoff between the system efficiency and EMF leakage should be considered. Especially for the power transfer of long-distance portable electronics, efficiency and EMF safety are the most important qualifications.

Most papers have studied methods of enhancing system efficiency. O. Jonah et al proposed that high quality coils can ensure effective energy transmission [8]. However, more design considerations are required. In addition, the influence of the intermediate coil on the efficiency of the WPT system has been discussed in detail in [9]. Note that the intermediate coils can affect the actual application in many cases. In [10], [11], a PCB coil with capacitive compensation was proposed to solve the planar or lateral misalignments. However, the EMF leakage of the system was not discussed or studied. Currently, most papers have studied the properties of the evanescent wave amplification of negative-permeability metamaterial (NPM), which can increase the system efficiency and alleviate the coil offset [12]-[15]. However, most studies are devoted to studying the NPM located between

The associate editor coordinating the review of this manuscript and approving it for publication was Wei E. I. Sha.

the transmitter and receiver. Furthermore, the NPM mainly occupies the transmission path of the system, and the presence of an additional structure will directly impact the WPT application.

Metal, ferrite and the zero-permeability metamaterial (ZPM) have been proposed to shield the leaking magnetic field [16]–[18]. In [17], a metal plate that is vertical to the coil is proposed to enhance the efficiency and achieve lower EMF leaking. However, the metal and ferrite material can shield the magnetic field of all the bands, including the desired signals. In [15], [18], the position of the ZPM above the coils (parallel to the coils) was proposed. In addition to the EMF leakage of the transmitter and receiver, the EMF leakage in the transmission path should also be considered. Moreover, the performance of the side-placed ZPM has not been proposed. The comparison of the side-placed ZPM and side-placed aluminum has not been investigated. In addition, an analytical model of the combination of side-placed NPMs and ZPMs has not been presented.

Currently, the effect of an EMF field on the human body has been widely investigated [19], [20], the EMF induced by the WPT coils cannot be ignored. Therefore, the EMF exposure level should comply with the International Commission on Nonionizing Radiation Protection [21], [22]. In reality, when WPT technology is applied to supply power to equipment, we need to consider a method of enhancing the efficiency while simultaneously meeting EMF safety requirements while not affecting the wireless transmission path. In reality, when the WPT technology is applied to supply the power to the equipment, we need to consider a method to enhance efficiency and human safety at same time, while not affecting the wireless transmission path. Especially, the advantage of side-placed metamaterial is that it will not disturb the energy transmission channel of the WPT system. Therefore, the transmission properties of two kinds of side-placed metamaterials need to be studied.

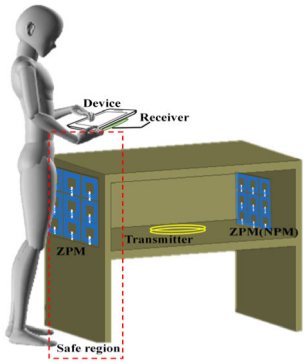


**FIGURE 1.** Scenario for device charging.

In this article, novel side-placed metamaterials are presented to simultaneously handle the low efficiency and high magnetic field leakage, as shown in Fig. 1. Through the simulation and experimental results, we show that the side-placed ZPM slabs and the combination of NPM and ZPM slabs are excellent choices for increasing efficiency and complying with the low EMF exposure requirements. Meanwhile, this combination can prevent the misalignment of the coils. And the side-placed system can prevent electromagnetic radiation interference between the devices. In comparison with aluminum plate, the ZPM slab offers better efficiency improvement and leakage EMF reduction.

The paper is organized as follows. The model and the working principles of the WPT system with the NPM and ZPM are introduced in Section II. In Section III, the performance of the NPM, ZPM, and the combination of NPM and ZPM slabs are analyzed through simulations and experiments. Furthermore, the performance of the ZPM slab is compared with that of aluminum. Finally, we summarize the conclusions.

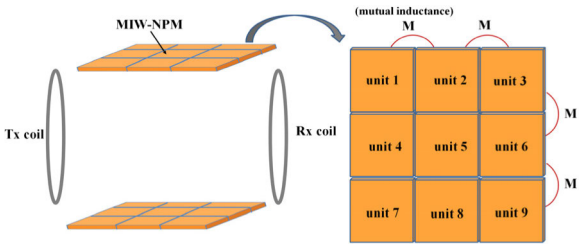


**FIGURE 2.** Configuration of the side-placed NPM slabs in WPT system.

## II. MODELING OF THE METAMATERIAL

### A. PRINCIPLE OF THE METAMATERIAL

When the side-placed NPM slabs are vertical to the system, the ability to propagate magneto-inductive waves (MIWs) has been shown, resulting in the enhancement of the efficiency [23]–[27]. The principle of the side-placed NPM slabs that are vertical to the coils is shown in Fig. 2. The magnetic field excited from the unit cell can pass through the neighboring unit cell, so the coupling effect occurs, and the MIW propagation is generated. It can be concluded that the energy transmitted by the Tx coil is obtained by the Rx coil because the MIW propagates in NPM slabs. Therefore, the efficiency can be improved when the two NPM slabs are placed in the left and right regions of the energy transmission path.

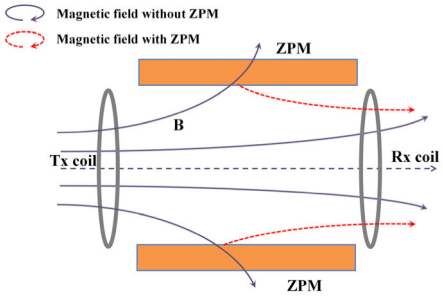


**FIGURE 3.** Transmission model of the proposed side-placed ZPM slabs.

Fig. 3 illustrates the propagation rule of the side-placed ZPM slabs in WPT system. It is shown that the magnetic

fields between the air and ZPM are almost prohibited, and the magnetic fields in the transport channel of the WPT system are converging to the Rx coil. Thus, it is very useful for the side-placed ZPM slabs to enhance the efficiency, while maintaining the safety.

Since the concept of MIWs was proposed in the NPM slab, its scattering characteristics have been analyzed in detail [23], [24].

The wave number ($k$) is $k = \beta - i\alpha$, where $\beta$ represents the propagation factor, and $\alpha$ is attenuation factor. The propagation of the unit cell at resonant frequency ($\omega_0$) is described as follow:

$$\beta = \frac{1}{a}\arccos\left(\frac{\omega_0^2/\omega^2 - 1}{2\kappa_C}\right) \tag{1}$$

where $a$ is the distance between the cells, $\kappa_C$ ($\kappa_C = 2M/L$) is the coupling coefficient, $Q$ is quality factor, and $M$ and $L$ are the mutual inductance between the metamaterial structure and the self-inductance of the metamaterial, respectively.

In addition, the attenuation of the MIW is described by the dispersion equation in the system

$$\alpha = \frac{1}{2\kappa_C Q a \sin(\beta a)} \tag{2}$$

It is clear that the attenuation ($\alpha$) is related to $Q$ and $\kappa_C$. The attenuation can decrease with the increase in $Q$ and $\kappa_C$, which means that the loss of the metamaterial is low. As a result, the system efficiency of the ZPM with low attenuation can be greatly enhanced.

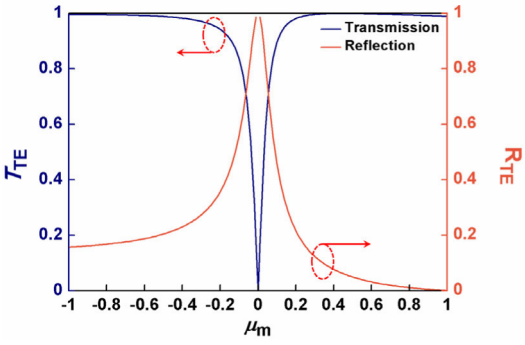


**FIGURE 4.** Calculated transmission and reflection of the metamaterial with $\mu_m$.

The transmission and reflection coefficients of the metamaterial model is calculated, as shown in (3), which can effectively demonstrate the working mechanism of the ZPM slab. Fig. 4 illustrates the analysis results of the two coefficients changing with the $\mu_m$. It can be found that the reflection coefficient of the wave is 1 and the transmission coefficient is 0 when the $\mu_m$ is equal to near zero, that is, the magnetic field is totally reflected.

$$T = \frac{e^{-i\sqrt{k_0^2-k^2}t}}{\cos\left(\sqrt{k_0^2-\frac{k^2}{\mu_m}}t\right) - i\left(\frac{2k_0^2\mu_m - k^2(\mu_m+1)}{2\mu\sqrt{(k_0^2-\frac{k^2}{\mu_m})(k_0^2-k^2)}}\right)\sin\left(\sqrt{k_0^2-\frac{k^2}{\mu_m}}t\right)}$$

$$R = \frac{\frac{-ik^2}{\mu_m}\sin\left(\sqrt{k_0^2-\frac{k^2}{\mu_m}}t\right)}{\cos\left(\sqrt{k_0^2-\frac{k^2}{\mu_m}}t\right) - i\left(\frac{2k_0^2\mu_m - k^2(\mu_m+1)}{2\mu\sqrt{(k_0^2-\frac{k^2}{\mu_m})(k_0^2-k^2)}}\right)\sin\left(\sqrt{k_0^2-\frac{k^2}{\mu_m}}t\right)} \tag{3}$$

where $k_0$ is the wavenumber in vacuum, $k$ represents the wave number parallel to the metamaterial, and $t$ is the thickness of the metamaterial.

### B. MODELING OF THE SYSTEM

The WPT system consists of two elements: the transmitter and receiver, which consist of the source coil, Tx coil, load coil and Rx coil. The diameters of the coils are both 20cm. The Tx and Rx coils are tuned to the frequency of the 13.56MHz ISM band, and the resonance frequency of the coils is carefully tuned by the lumped capacitance. The unit cells of the NPM and ZPM are both realized with a square spiral resonator, and the size of the unit cell is 12cm × 12cm [15]. The operating frequencies of the NPM and ZPM are changed by using the external capacitor. The sizes of the NPM and ZPM slabs are both 36cm × 36cm. The slabs are vertical to the coils and parallel to the transport channel.

In fact, the metamaterial can be represented by an equivalent circuit model (including equivalent inductance ($L$), capacitance($C$), and resistance ($R$)). Thus, in order to accurately obtain the equivalent permeability of the NPM and ZPM, the equivalent circuit model is used to calculate the $L$, C and R. And, the electromagnetic parameter of the metamaterial is extracted by (4).

$$\mu_m = 1 - F\left(1 - \frac{1}{w^2 LC} - \frac{R}{jwL}\right)^{-1} \tag{4}$$

The inductance, capacitance and resistance of the square spiral are written as [28], [29]:

$$L = \frac{1.27\mu_0 N^2 d_{ad}}{2}\left[\ln\left(\frac{2.07}{\phi}\right) + 0.18\phi + 0.13\phi^2\right] \tag{5}$$

where $N$ represents the number of spiral turns, $d_{ad}$ is the average diameter of the spiral coil, and $\Phi$ is the fill factor.

$$C = (0.9 \times 1 + 0.1 \times 4.4)\varepsilon_0 \frac{t}{s} l + C_l \tag{6}$$

where $l$ is the total length of gap, $s$ is the spacing between the turns, and $C_l$ is the capacitor of the lumped capacitor.

$$R = R_{dc}\frac{t}{\delta(1-e^{-t/\delta})} + 0.1R_{dc}\left(\frac{\mu_0 w_0 w^2}{0.434(s+w)}\right) + R_0 + \frac{\tan\delta}{w_0 C} \tag{7}$$

where $R_{dc}$ is the dc resistance, $R_0$ is the resistance of the lumped capacitor, $w$ is the width, and $\delta$ is the skin depth,.

Fig. 5 shows the comparison of the calculated and measured permeability results. From the results, it can be concluded that the analyzed permeability and measured permeability are in agreement. When the external capacitor is 95pf and 120pf, the effective permeability values of the NPM

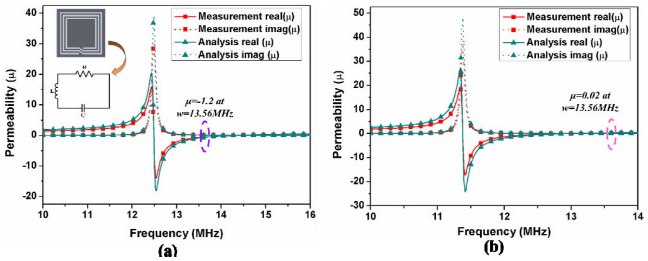


**FIGURE 5.** Permeability of the metamaterial (a) NPM (b) ZPM.

**TABLE 1.** Specifications of the square spiral.

| | line width | turn spacing | outer diameter | inner diameter |
|---|---|---|---|---|
| (mm) | 4 | 3 | 120 | 73 |

and ZPM are near -1 and 0.02 at 13.56MHz, respectively. Table 1 lists the final parameters of the metamaterial.

Three system models are built to study the transfer and magnetic field characteristics to determine the optimal combination scheme of the WPT system, as shown in Fig. 6. The two NPM slabs, the two ZPM slabs, and the combination of the NPM and ZPM slabs in the system are referred to as Type A, Type B, and Type C, respectively. The metamaterials have a vertical displacement from the central axis with a distance of $D_1$ (vertical distance). The axial distance between the Tx coil and the Rx coil is defined as D.

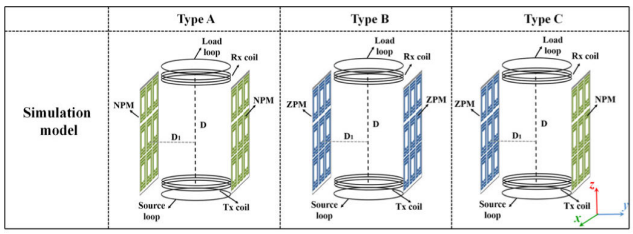


**FIGURE 6.** Three system models of the side-placed NPM slabs, ZPM slabs, and combination of the NPM and ZPM slabs.

## III. SIMULATION AND EXPERIMENTAL OF THE SYSTEM INTEGRATION

### A. SIMULATION RESULTS FOR THE SIDE-PLACED METAMATERIAL

The simulated magnetic field results of the proposed system models are shown in Fig. 7, where D is fixed at 40cm. The vertical distance from the metamaterial to the center axis is set to D1=17cm. Fig. 7(a) shows the simulated result for the case of original system without metamaterial. The magnetic field distributions simulated in Types A, B and C are presented in Fig. 7(b)-7(d). The results show that the field strength of the Rx coil is enhanced in the proposed three cases compared to Fig. 7(a). However, it can be observed that the field distribution behind the NPM slab in type A increases compared to the simulated results of the system without the metamaterial. Besides, it is worthwhile to note that the field

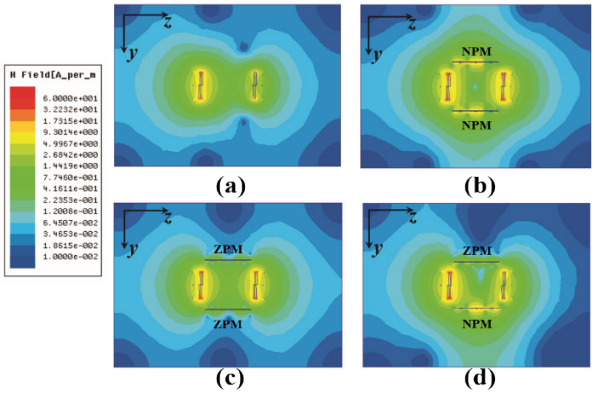


**FIGURE 7.** Field distribution (a) original system, (b) NPM slabs, (c) ZPM slabs, and (d) combination of NPM and ZPM slabs.

strength outside the ZPM slab is reduced and the magnetic field around the Rx coil is improved in type B. The magnetic field in type C is reduced on one side and increased on the other side. In Section III B, the performance of the NPM and ZPM slabs in the system is discussed in detail.

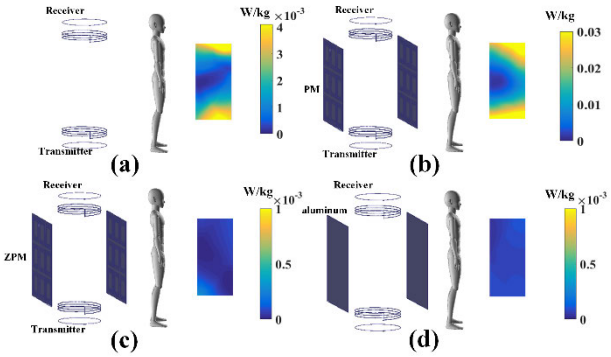


**FIGURE 8.** SAR simulation (13.56MHz): (a) original system, (b) with NPM slabs, (c) with ZPM slabs, and (d) with aluminum plates.

In general, aluminum is applied as magnetic shielding for the WPT system. And we use the aluminum plate to compare to the metamaterials. The size of the aluminum plate is identical to the metamaterial and it is located at the same position. To explore the effect of the NPM slabs, ZPM slabs and aluminum plates on humans, a box is established to simulate human body tissue. The parameter of the box is chosen as the cerebrospinal fluid, where the conductivity and relative permittivity are 2.0041 and 108.26, respectively. Fig. 8 shows the 10-g average specific absorption rate (SAR) in the four cases. The distance from the box to the center of the coil is 25cm. Fig. 8(a)-(d) shows the exposure scenarios of the original system, the system with NPM slabs, the system with ZPM slabs, and the system with the aluminum plate. The SAR values are $4 \times 10.3$ W/kg, $3 \times 10.2$ W/kg, $0.07 \times 10.3$ W/kg, and $0.1 \times 10.3$ W/kg. It is illustrated that the side-placed ZPM slab can mitigate the EMF, and lower the EMF exposure levels. And the SAR of the system with the ZPM slab is less than that of the aluminum.

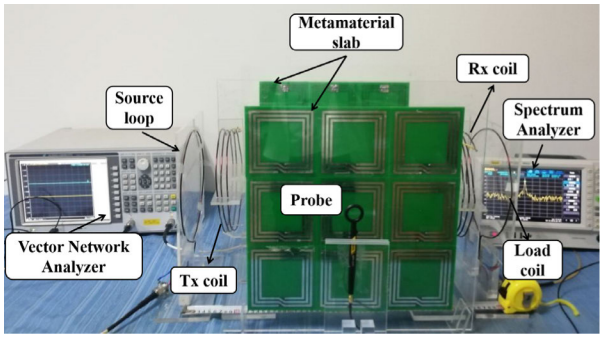


**FIGURE 9.** Experimental prototype of the side-placed metamaterial.

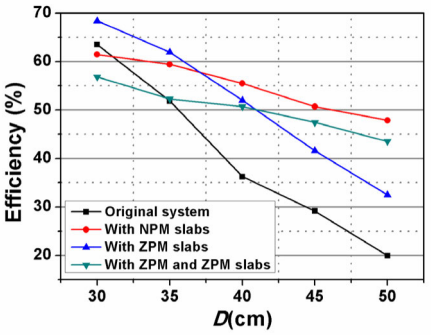


**FIGURE 10.** Relationship between the measured efficiency and transfer distance D.

### B. MEASUREMENT RESULTS OF EFFICIENCY

In this chapter, we discuss the experimental verification of the WPT with NPM and ZPM slabs. It is worth noting that the dimensions of the experimental device are the same as those of the model in the electromagnetic simulation. Fig. 9 shows the implemented WPT charging system with the metamaterials. The coils in the WPT system are fabricated with a copper wire that is 1.25mm in thickness and 20cm in diameter. The Tx and Rx coils are carefully tuned to achieve resonance at 13.56MHz. The overall size of the $3 \times 3$ array of the NPM and ZPM slabs are 36cm$\times$36cm. Each metamaterial is measured to ensure that the effective permeability is at -1 and near-zero at 13.56MHz.

To verify the proposed model, we measured the efficiency and the magnetic field. The vector network analyzer (VNA-AV-3656A) can be used to supply a signal to the Tx coil. The transmission coefficient $S_{21}$ is measured after the standard two-port calibration. The spectrum analyzer (RSA3030-TG) and the probe are used to measure the magnetic field. In order to ensure the effectiveness of the experiment, we first measured the efficiency of the original system, and then we measured the power transfer efficiency and leaked magnetic field of the three designed models.

The resistances of the source and load are assumed to be 50Ω [30]. In the tests, the distance from the source to Tx coil and load to Rx coil are changed to achieve the impedance matching [31]. Therefore, $|S_{21}|^2$ can be used to calculate the system efficiency in this article.

$$\eta = |S_{21}|^2 \times 100\% \tag{8}$$

To determine the available range of the system with the metamaterials, the system efficiency varies with the transfer distance D is discussed. During the measurement, the Tx coil is fixed and the metamaterials are placed on the sides at 17cm. Fig. 10 shows the efficiency varying with D. From the results, we can see that the ZPM slabs can increase the efficiency at all distances. However, the system efficiency is rapidly reduced as the distance D increases. When the NPM slab is used at D = 30cm, the system efficiency is lower compared to the original system due to the high loss of the NPM at the short distance. And the NPM slabs can enhance the efficiency as the transfer distance increases. In addition, it can be found that the efficiency of the combination of the NPM and ZPM slabs is still lower than that of the NPM slabs as D increases. Furthermore, it is obvious that the efficiency of the combination of the NPM and ZPM slabs is higher than that of the ZPM slabs when D exceeds 40cm, which can mitigate the efficiency reduction. The reasons for the above performance of the different metamaterial systems: 1) the magnetic field reflected by the ZPM is attenuated with the transfer distance increased, and most magnetic fields are not received by the receiver. 2) the efficiency improvement of the NPM is due to the MIW, and the efficiency drops slowly as the transfer distance increases. 3) the reflected magnetic field can act on the NPM slabs and disturb the MIW.

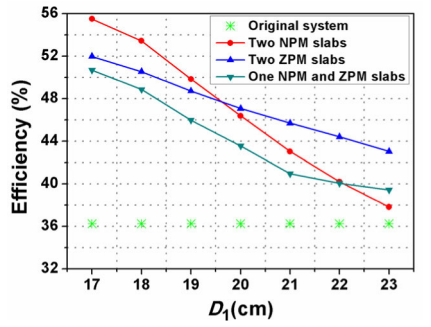


**FIGURE 11.** Measured efficiencies for different combinations of metamaterials.

To understand how to enhance the WPT efficiency of the side-placed NPM and ZPM slabs, the efficiency versus the vertical distance $D_1$ is investigated at D = 40cm. The efficiency results of the three system models are measured, as shown in Fig. 11. During the measurement, the vertical distance $D_1$ increases from 17cm to 23cm. It can be seen that the system efficiency drops quickly as $D_1$ increases when the NPM slabs are used. The efficiency varies relatively smoothly when two ZPM slabs are applied in the system. Moreover, the combination of the NPM and ZPM slabs can lessen the decreasing tendency of the efficiency. When the NPM slabs, ZPM slabs, and the combination of the NPM and ZPM slabs are used, the efficiency drops from 55.5% to 37.8% (17.7%), 52% to 43% (9%), and 51% to 39.5% (11.5%). Therefore,

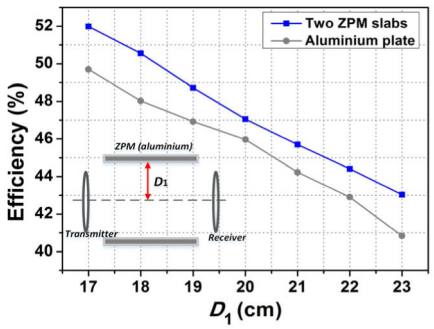


**FIGURE 12.** Measured system efficiency of the ZPM slabs and aluminum plate.

the ZPM slabs and the combination NPM and ZPM slabs are suitable for the large vertical distance ($D_1$). Fig. 12 illustrates the efficiency comparison of system with the aluminum and ZPM slabs. In the measurement of the vertical distance from 17cm to 23cm, the efficiency of the system with the ZPM slab is higher than that of the aluminum plate.

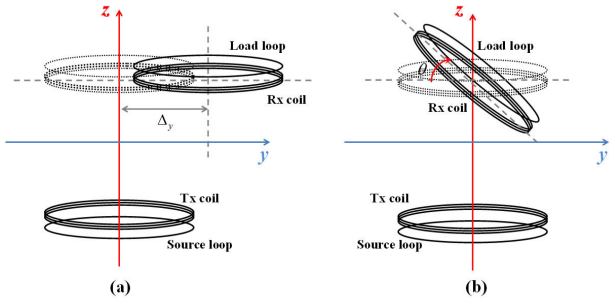


**FIGURE 13.** Schematic of the Rx coil offset. (a) Misalignment 1 (lateral misalignment). (b) Misalignment 2 (angular misalignment).

In what follows, the effects of the lateral and angular misalignments of the Rx coil on the efficiency are investigated. The sketches of the misalignments of the proposed WPT are shown in Fig. 13. Fig. 13(a) shows the lateral misalignment of the receiver which is referred to as misalignment 1. Herein, the transmitter and receiver are located in parallel plane of *xoy*, and the receiver is offset along the y axis (the distance from the center axis is $\Delta$y). Misalignment 2 is the angular misalignment of the receiver, as shown in Fig. 13(b). The receiver is rotated around the x axis with an angle of $\theta$. As we all know, the efficiency drops rapidly for the misalignments of the coils. Methods for mitigating the influence of the misalignment of the metamaterial slabs on both sides of the coils are discussed.

Owing to the movable range limitation of the Rx coil at short transfer distance, the misalignments of the Rx coil are discussed at D = 50cm. A comparison of the efficiencies with the various lateral misalignments is illustrated in Fig. 14(a). The lateral misalignment varies from 0 to 14cm in steps of 2cm. The maximum efficiency of the original system at D = 50cm is 19.98% when the coils do not exhibit lateral misalignment. When two NPM (ZPM) slabs are used,

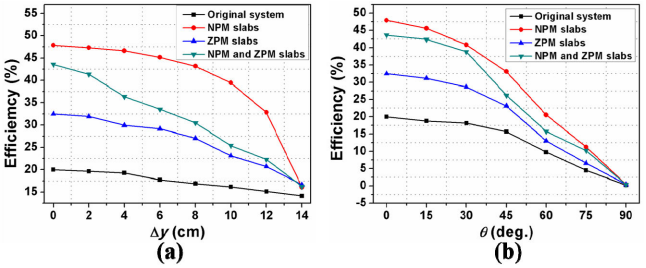


**FIGURE 14.** Measurement efficiencies of the WPT system with various misalignment. (a) lateral misalignment $\Delta y$. (b) angular misalignment $\theta$.

the system efficiency improves to 47.89% (32.49%) with $\Delta$y = 0 and D = 50cm. The system efficiency is increased to 43.56% when the combination of NPM and ZPM slabs is applied. From the results, it is worthwhile to point out that the efficiency still improves compared to the original system even the large lateral misalignment ($\Delta$y = 14cm). Even with a large lateral misalignment of $\Delta$y = 12cm, the efficiency of the three cases is still higher than that of the original WPT system without lateral misalignment.

Fig. 14(b) shows the measured efficiencies for angular misalignment variation. Decreased efficiencies are clearly observed as $\theta$ increases. However, compared to the original system, the efficiency increases substantially when the metamaterial slabs are used. At $\theta = 60°$, the efficiency of NPM system model is higher than that of the original system at $\theta = 0°$. The efficiency of ZPM system model and the combination of NPM and ZPM slab system model is higher than that of the original system at $\theta = 45°$. Besides, the system efficiency is near zero at angular misalignment of $\theta = 90°$, regardless of the system with and without metamaterial slabs. The reason for this phenomenon is the weak coupling between the coils. In practice, the lateral and angular misalignment are usually small for the most WPT applications. Therefore, it is clear that the side-placed ZPM slab and NPM slab can mitigate the effect of misalignment on the performance of system.

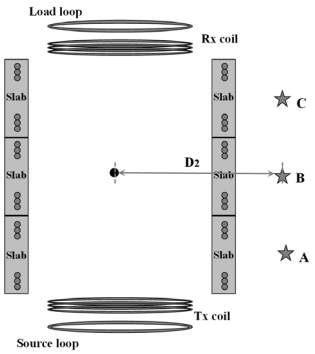


**FIGURE 15.** Measurement positions for the magnetic field.

### C. MEASUREMENTS RESULTS OF MAGNETIC FIELD

Apart from the study of the efficiency, the leakage EMF of the WPT system should be investigated. Fig. 15 shows the measurement schematics of the WPT system. To demonstrate the

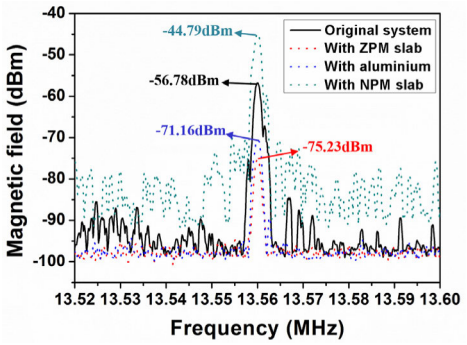


**FIGURE 16.** Measurement results of the WPT system at $D_2 = 25$cm.

effectiveness of the two kinds of metamaterials, we measured the EMF strength of point B, which is 25cm away from the axis, as shown in Fig. 16. The transfer distance D is fixed at 40cm, and $D_1$ is fixed at 17cm. We measured the EMF strength in the four cases: the original system, the system with ZPM slab, the system with alunimium and the system with NPM slab. The experimental results show that the EMF strength of original system is -56.78dBm, and the magnetic field strength is -75.23dBm when the ZPM slab is applied. The EMF strength is reduced by 18.45dBm due to the effect of the ZPM slab. Moreover, it is clear that the EMF strength of ZPM slab is lower than that of aluminum. We can draw the conclusion that the shielding performance of the ZPM slab is better than the aluminum. In addition, it is shown that the EMF strength in the case of system with NPM slab is higher compared to original system. Because of the strong MIW on the surface of NPM, the EMF strength is enhanced around the side of the coils when the NPM slab is used.

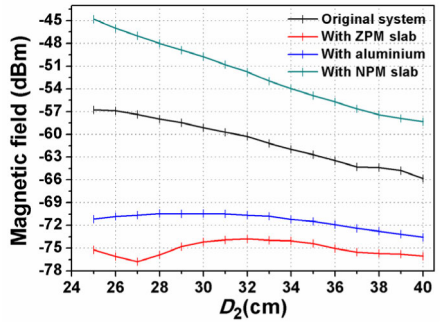


**FIGURE 17.** Magnetic field depending on the measured points.

Fig. 17 shows the measured results when the distance of the point B changes. The distance between the measured point and the center axis is $D_2$. The results show that the magnetic fields behind the ZPM slab and aluminum are reduced, and the NPM slab is enhanced compared to the original system at all measured points. And the magnetic field behind the ZPM slab is still lower than that of the aluminum as $D_2$ varies.

Besides, three points are selected in the same plane at the distance $D_2$ of 25cm. The results of the EMF strength at A, B and C are given in Table 2. As a result, the magnetic fields of the ZPM system model and NPM system model

**TABLE 2.** Measured magnetic field strength of the points.

| Solution | A | B | C |
|---|---|---|---|
| Original system | -53.74 dBm | -56.78 dBm | -51.9 dBm |
| With ZPM | -69.14 dBm | -75.23 dBm | -68.71 dBm |
| With aluminum | -65.29 dBm | -71.16 dBm | -64.86 dBm |
| With NPM | -42.41 dBm | -44.79 dBm | -40.36 dBm |

at three points are reduced and enhanced, respectively. The experimental results verify the simulation magnetic field distribution, and indicate that the research method is valid.

The WPT system with the side-placed metamaterial in this article has competitive advantages. First, it does not affect the channel of the energy transfer. Besides, the side-placed metamaterials have two functions: increasing the efficiency and reducing the leakage EMF in the horizontal area. Based on the above analysis of the efficiency and magnetic field, different types of metamaterials have different electromagnetic transmission characteristics. The ZPM slabs and the combination NPM and ZPM slabs can achieve the good performance. Since the combination of NPM and ZPM slabs only reduces the leakage electromagnetic field (EMF) on one side, it can be applied for the situation where the demand for the magnetic field leakage is not high. Two ZPM slabs are more suitable for the low EMF requirement. In our proposed system, the combination of NPM and ZPM slabs is selected when the transfer distance is larger than 40cm. When the transfer distance is lower than 40cm, the two ZPM slabs are a good choice.

## IV. CONCLUSION

This article proposed a solution that uses the side-placed NPM and ZPM slabs in a WPT system to simultaneously obtain high efficiency and a low human exposure value in the unintended area. Moreover, there are no additional obstacles for the energy transmission between the coils when the side-placed metamaterials are vertical to the system, which lays a good foundation for the practical application of the wireless charging. The measured results for a fabricated structure showed that the proposed WPT system with different types of metamaterials achieved good efficiency improvement to a certain extent. When the transfer distance exceeds 40cm (under 40cm), the combination of the NPM and ZPM slabs in the WPT system (two ZPM slabs) has good performance. The side-placed metamaterials have a prospect for solving the lateral and angular misalignment of the coil. Additionally, the measurement results show that the EMF strength outside the ZPM slab is decreased and the shielding performance is better than that of aluminum plate. The proposed structure can be applied to an area with multiple WPT charging systems, and consumer devices.

## REFERENCES

[1] Z. Zhang, H. Pang, A. Georgiadis, and C. Cecati, "Wireless power transfer—An overview," *IEEE Trans. Ind. Electron.*, vol. 66, no. 2, pp. 1044–1058, Feb. 2019.

[2] A. Kurs, A. Karalis, R. Moffatt, J. D. Joannopoulos, P. Fisher, and M. Soljačić, "Wireless power transfer via strongly coupled magnetic resonances," *Science*, vol. 317, no. 5834, pp. 83–86, Jul. 2007.

[3] L. Li, H. Liu, H. Zhang, and W. Xue, "Efficient wireless power transfer system integrating with metasurface for biological applications," *IEEE Trans. Ind. Electron.*, vol. 65, no. 4, pp. 3230–3239, Apr. 2018.

[4] W. Lin, R. W. Ziolkowski, and J. Huang, "Electrically small, low profile, highly efficient, huygens dipole rectennas for wirelessly powering Internet-of-Things (IoT) devices," *IEEE Trans. Antennas Propag.*, vol. 67, no. 6, pp. 3670–3679, Jun. 2019.

[5] P. S. Riehl, A. Satyamoorthy, H. Akram, Y.-C. Yen, J.-C. Yang, B. Juan, C.-M. Lee, F.-C. Lin, V. Muratov, W. Plumb, and P. F. Tustin, "Wireless power systems for mobile devices supporting inductive and resonant operating modes," *IEEE Trans. Microw. Theory Techn.*, vol. 63, no. 3, pp. 780–790, Mar. 2015.

[6] F. Musavi and W. Eberle, "Overview of wireless power transfer technologies for electric vehicle battery charging," *IET Power Electron.*, vol. 7, no. 1, pp. 60–66, Jan. 2014.

[7] H. Kim, C. Song, J. Kim, J. Kim, and J. Kim, "Shielded coil structure suppressing leakage magnetic field from 100W-class wireless power transfer system with higher efficiency," in *IEEE MTT-S Int. Microw. Symp. Dig.*, May 2012, pp. 83–86.

[8] O. Jonah, S. V. Georgakopoulos, and M. M. Tentzeris, "Optimal design parameters for wireless power transfer by resonance magnetic," *IEEE Antennas Wireless Propag. Lett.*, vol. 11, pp. 1390–1393, Dec. 2012.

[9] F. Zhang, S. A. Hackworth, W. Fu, C. Li, Z. Mao, and M. Sun, "Relay effect of wireless power transfer using strongly coupled magnetic resonances," *IEEE Trans. Magn.*, vol. 47, no. 5, pp. 1478–1481, May 2011.

[10] L. L. Pon, S. K. Abdul Rahim, C. Y. Leow, M. Himdi, and M. Khalily, "Displacement-tolerant printed spiral resonator with capacitive compensated-plates for non-radiative wireless energy transfer," *IEEE Access*, vol. 7, pp. 10037–10044, Jan. 2019.

[11] L. L. Pon, C. Y. Leow, S. K. Abdul Rahim, A. A. Eteng, and M. R. Kamarudin, "Printed spiral resonator for displacement-tolerant near-field wireless energy transfer," *IEEE Access*, vol. 7, pp. 172055–172064, Jan. 2019.

[12] B. Wang, K. H. Teo, T. Nishino, W. Yerazunis, J. Barnwell, and J. Zhang, "Experiments on wireless power transfer with metamaterials," *Appl. Phys. Lett.*, vol. 98, no. 25, Jun. 2011, Art. no. 254101.

[13] A. Ranaweera, T. P. Duong, and J. W. Lee, "Experimental investigation of compact metamaterial for high efficiency mid-range wireless power transfer applications," *J. Appl. Phys.*, vol. 116, no. 4, pp. 83–86, Jul. 2014.

[14] Y. Cho, S. Lee, D.-H. Kim, H. Kim, C. Song, S. Kong, J. Park, C. Seo, and J. Kim, "Thin hybrid metamaterial slab with negative and zero permeability for high efficiency and low electromagnetic field in wireless power transfer systems," *IEEE Trans. Electromagn. Compat.*, vol. 60, no. 4, pp. 1001–1009, Aug. 2018.

[15] C. Lu, C. Rong, X. Huang, Z. Hu, X. Tao, S. Wang, J. Chen, and M. Liu, "Investigation of negative and near-zero permeability metamaterials for increased efficiency and reduced electromagnetic field leakage in a wireless power transfer system," *IEEE Trans. Electromagn. Compat.*, vol. 61, no. 5, pp. 1438–1446, Oct. 2019.

[16] S. C. Tang, S. Y. Hui, and H. S.-H. Chung, "Evaluation of the shielding effects on printed-circuit-board transformers using ferrite plates and copper sheets," *IEEE Trans. Power Electron.*, vol. 17, no. 6, pp. 1080–1088, Nov. 2002.

[17] L. Huang, J. Zou, Y. Zhou, Y. Hong, J. Zhang, and Z. Ding, "Effect of vertical metal plate on transfer efficiency of the wireless power transfer system," *Energies*, vol. 12, no. 19, p. 3790, Oct. 2019.

[18] J. Besnoff, M. Chabalko, and D. S. Ricketts, "A frequency-selective zero-permeability metamaterial shield for reduction of near-field electromagnetic energy," *IEEE Antennas Wireless Propag. Lett.*, vol. 15, pp. 654–657, Aug. 2016.

[19] M. Koohestani, M. Ettorre, and M. Zhadobov, "Local dosimetry applied to wireless power transfer around 10 MHz: Dependence on EM parameters and tissues morphology," *IEEE J. Electromagn., RF Microw. Med. Biol.*, vol. 2, no. 2, pp. 123–130, Jun. 2018.

[20] X. L. Chen, A. E. Umenei, D. W. Baarman, N. Chavannes, V. D. Santis, J. R. Mosig, and N. Kuster, "Human exposure to close-range resonant wireless power transfer systems as a function of design parameters," *IEEE Trans. Electromagn. Compat.*, vol. 56, no. 5, pp. 1027–1034, Oct. 2014.

[21] International Commission on Non-Ionizing Radiation Protection, "Guidelines for limiting exposure to time-varying electric and magnetic fields (1 Hz to 100kHz)," *Health Phys.*, vol. 99, no. 6, pp. 818–836, 2010.

[22] A. Ahlbom *et al.*, "Guidelines for limiting exposure to time-varying electric, magnetic, and electromagnetic fields (up to 300 GHz) (international commission on non-ionizing radiation protection)," *Health Phys.*, vol. 74, no. 4, pp. 494–522, Apr. 1998.

[23] E. Shamonina, V. A. Kalinin, K. H. Ringhofer, and L. Solymar, "Magnetoinductive waves in one, two, and three dimensions," *J. Appl. Phys.*, vol. 92, no. 10, pp. 6252–6261, Nov. 2002.

[24] C. J. Stevens, "Power transfer via metamaterials," *Comput. Mater. Continua*, vol. 33, no. 1, pp. 1–18, 2013.

[25] C. J. Stevens, "Magnetoinductive waves and wireless power transfer," *IEEE Trans. Power Electron.*, vol. 30, no. 11, pp. 6182–6190, Nov. 2015.

[26] F. S. Sandoval, A. Moazenzadeh, and U. Wallrabe, "Comprehensive modeling of magnetoinductive wave devices for wireless power transfer," *IEEE Trans. Power Electron.*, vol. 33, no. 10, pp. 8905–8915, Oct. 2018.

[27] F. S. Sandoval, S. M. T. Delgado, A. Moazenzadeh, and U. Wallrabe, "A 2-D magnetoinductive wave device for freer wireless power transfer," *IEEE Trans. Power Electron.*, vol. 34, no. 11, pp. 10433–10445, Mar. 2019.

[28] S. S. Mohan, M. del Mar Hershenson, S. P. Boyd, and T. H. Lee, "Simple accurate expressions for planar spiral inductances," *IEEE J. Solid-State Circuits*, vol. 34, no. 10, pp. 1419–1424, Oct. 1999.

[29] U.-M. Jow and M. Ghovanloo, "Modeling and optimization of printed spiral coils in air, saline, and muscle tissue environments," *IEEE Trans. Biomed. Circuits Syst.*, vol. 3, no. 5, pp. 339–347, Oct. 2009.

[30] G. Lipworth, J. Ensworth, K. Seetharam, D. Huang, J. S. Lee, P. Schmalenberg, T. Nomura, M. S. Reynolds, D. R. Smith, and Y. Urzhumov, "Magnetic metamaterial superlens for increased range wireless power transfer," *Sci. Rep.*, vol. 4, p. 3642, Jan. 2014.

[31] T. P. Duong and J.-W. Lee, "Experimental results of high-efficiency resonant coupling wireless power transfer using a variable coupling method," *IEEE Microw. Wireless Compon. Lett.*, vol. 21, no. 8, pp. 442–444, Aug. 2011.


**CONGHUI LU** was born in China, in 1994. She received the B.S. degree in physics from Zaozhuang University, China, in 2016, and the M.E. degree from the School of Physics, Huazhong University of Science and Technology, Wuhan, in 2019, where she is currently pursuing the Ph.D. degree with the State Key Laboratory of Advanced Electromagnetic Engineering and Technology. Her current research interest includes wireless power transfer systems using metamaterials.

**XIUTAO HUANG** was born in China, in 1990. He received the B.S. degree in physics from Zaozhuang University, Zaozhuang, China, in 2014, and the M.E. degree in plasma physics from the Huazhong University of Science and Technology, Wuhan, China, in 2017, where he is currently pursuing the Ph.D. degree with the State Key Laboratory of Advanced Electromagnetic Engineering and Technology. His current research interests include dielectric barrier discharge, metamaterials application, and metamaterial absorber.

**XIONG TAO** received the B.E. degree in applied physics from Shijiazhuang Tiedao University, Hebei, China, in 2017. He is currently pursuing the M.E. degree with the School of Electrical and Electronic Engineering, Huazhong University of Science and Technology, Wuhan, China. His current research interest includes wireless power transfer.

**CANCAN RONG** (Member, IEEE) was born in China, in 1991. He received the B.E. degree in electrical engineering and automation from Jiangsu Normal University, in 2014. He is currently pursuing the Ph.D. degree with the State Key Laboratory of Advanced Electromagnetic Engineering and Technology, Huazhong University of Science and Technology, Wuhan. His current research interest includes wireless power transfer systems using metamaterials.

**MINGHAI LIU** received the Ph.D. degree in physics from the University of Science and Technology of China, Hefei, China, in 1997. From 1997 to 1999, he was a Postdoctoral Fellow with the Institute of Plasma Physics, Chinese Academy of Sciences, Hefei. From 2002 to 2004, he was a Visiting Scholar with Nagoya University, Nagoya, Japan. Since 2000, he has been with the Huazhong University of Science and Technology, Wuhan, China, where he is currently a Professor with the State Key Laboratory of Advanced Electromagnetic Engineering and Technology. His research interests include metamaterials and wireless power transfer system for electric vehicle.